J Mater Sci (2009) 44:3608–3617
DOI 10.1007/s10853-009-3488-6

Formation of hexagonal close packing at a grain boundary in gold by the dissociation of a dense array of crystal lattice dislocations

D. L. Medlin · J. C. Hamilton

Received: 2 March 2009 / Accepted: 10 April 2009 / Published online: 28 April 2009

Abstract We analyze a thin ($\sim$1 nm) hexagonal-close-packed (HCP) intergranular layer at a 29° $\langle 110 \rangle$ tilt grain boundary in gold. Our analysis, which is based on HRTEM observations and atomistic calculations, shows that this boundary consists of a dense array of 60° $1/2\langle 110 \rangle$ crystal lattice dislocations that are distributed one to every two $\{111\}$ planes. These dislocations dissociate into paired Shockley partial dislocations, creating a stacking fault on every other plane and thereby producing the …*abab*…, or HCP, stacking sequence. This distribution of dislocations is consistent both with the measured intergranular misorientation and with the calculated rigid-body translation along the tilt axis. By establishing the interfacial dislocation arrangement, we also show how the HCP layer at the 29° boundary observed here is geometrically related to that found previously at the 80.6° $\Sigma = 43$ $\langle 110 \rangle$ boundary. This result helps to link dislocation-based descriptions for boundary structures between the high- and low-angle misorientation regimes.

Introduction

Grain boundaries in face-centered-cubic (FCC) metals with low stacking fault energies often form broad, three-dimensional structures that are composed of arrays of stacking faults [1–12]. A general question concerns how the pattern of such faults, and hence the structure of the boundary, is related to the orientational parameters that describe the macroscopic geometry of the interface. In this paper, we analyze the formation of a layer of hexagonal-close-packed (HCP) material at a grain boundary in gold. We present high-resolution transmission electron microscopy (HRTEM) observations and atomistic calculations of this interface. HCP has been predicted and observed previously at FCC grain boundaries [10–12], but at a higher misorientation than that of the boundary we analyze here. Thus, the specific questions we address here are: why does HCP form at this particular boundary and how is it related to the HCP that has been found at higher misorientations?

Our approach is to analyze the dislocations present at the interface. The misorientation of the boundary in this study, which is about 29°, falls in a limiting angular regime where the accommodation of misorientation by $1/2\langle 110 \rangle$ crystal lattice dislocations would require these dislocations to be spaced at atomic-scale separations. At such a close spacing, it is reasonable to ask whether such defects would retain any physical significance as individual entities. As we show here, despite the close spacing of the dislocations, the details of the interfacial structure and its relationship to the intergranular misorientation can be understood in terms of the properties of the individual dislocations present at the interface. Specifically, the HCP stacking arises through the dissociation of a dense array of crystal lattice dislocations into pairs of Shockley partial dislocations that produce stacking faults on alternating $\{111\}$ planes. Furthermore, by establishing the details of this dislocation arrangement, we show how the formation of HCP at this boundary is related to the HCP intergranular layers that have been found previously at boundaries of higher misorientation [10, 12].

D. L. Medlin (✉) · J. C. Hamilton
Sandia National Laboratories, Livermore, CA 94551, USA
e-mail: dlmedli@sandia.gov

Experimental procedure

The boundary investigated in this paper was observed in a thin film of gold. We investigated gold because its low stacking fault energy ($\sim$33 mJ/m^2 [13, 14]) allows dislocations to spread into dissociated configurations and because it is straightforward to prepare thin film samples that have a $\langle 110 \rangle$ crystallographic texture, an orientation that is convenient for detailed, atomic-scale analysis of the dislocation arrangements. We vapor deposited gold onto a polished, $\langle 110 \rangle$-oriented, single-crystal NaCl substrate ($T = 300°$). Growth on this substrate yields a film with a strong $\langle 110 \rangle$ texture. In addition to epitaxial and twin-oriented grains, a number of non-twin-related $\langle 110 \rangle$ tilt boundaries, such as the boundary analyzed here, arise in these films. After growth, the NaCl substrate was dissolved in de-ionized water, and the remaining film was collected on a fine-meshed grid. The supported film was then thinned to electron transparency using Ar+ ion milling and examined in a JEOL 4000EX HRTEM operated at 400 kV. The misorientation and inclination of the boundary were measured by analyzing the HRTEM intensity peak positions, which were extracted from the HRTEM image using a peak finding algorithm in the commercial software package MacTempas (Total Resolution LLC, Berkeley, CA, 94707, USA).

Results

An overview of the grain boundary analyzed in this paper and several of its neighbors is shown in Fig. 1; an enlargement of the dissociated region of boundary, which is indicated by the bracket, is shown in Fig. 2. The boundary lies near a 5-fold {111} twin junction, which is located at the lower right side of the image. Near the bottom of the image, the boundary intersects one of the {111} twins that radiate out from this twin junction. Above the indicated region of boundary, which is about 60 Å long, the contrast from the boundary becomes more complex and difficult to interpret. This change in contrast may reflect a rotation of the boundary inclination, through the thickness of the film, away from the $\langle 110 \rangle$ zone.

Over the indicated section, the boundary possesses a broad, dissociated core, as is evident from the gradual bending of the (111) planes as they cross the boundary. In this region, the boundary has a repeating pattern with a periodicity of two planes. As shown in the enlargement at the right of Fig. 2, this repeat pattern is consistent with the …*abab*… stacking arrangement of close-packed planes in a hexagonal-close-packed (HCP) structure.

To investigate the relationship of this structure to the geometry of the boundary, we measured the misorientation and inclination of the boundary. To make these measurements, we analyzed the positions of lattice fringe intensity peaks extracted from the HRTEM image (Fig. 3). By fitting lines to the intensity peaks along the (111) planes on either side of the interface, we measured a misorientation of 28.8 ± 0.5° about the $\langle 110 \rangle$ tilt axis. To measure the boundary inclination, we first computed the local angle of each (111) plane as a function of distance along the plane. We measured this angle at each peak by fitting a line to the peak and its two adjacent neighbors on a given (111) plane. We then defined the boundary position at each (111) plane as the peak position with a local angle closest to the midpoint of the far-field angles on the two sides of the interface. A line fit to the boundary positions gives an average inclination of 16.1° relative to [111] in the left crystal (and 12.7° relative to the [111] in the right crystal).

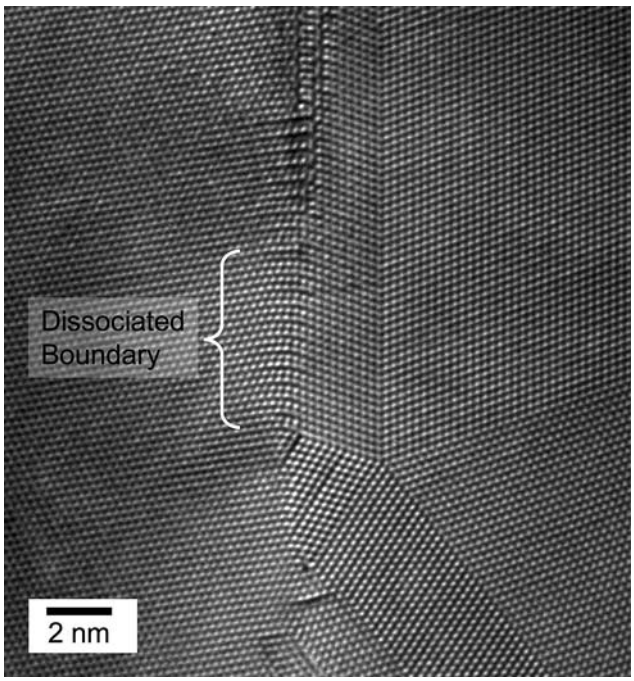

Fig. 1 HRTEM image giving an overview of the dissociated grain boundary and its neighbors

Inspection of the boundary positions, which are marked on Fig. 3, shows that this section of boundary is composed of two terraces that lie parallel to $(1\bar{3}1)$ in the left crystal and $(1\bar{1}1)$ in the right crystal and are separated by a step of one $(1\bar{1}1)$ plane height. As we discuss in the appendix, additional insight concerning the role of these steps is provided by analyzing the boundary in a coherent reference frame for which $(1\bar{3}1)$ and $(1\bar{1}1)$ are parallel. The dislocation content of this type of step (or disconnection) accommodates the strain required to ensure coherency of the (111) planes crossing this interface.

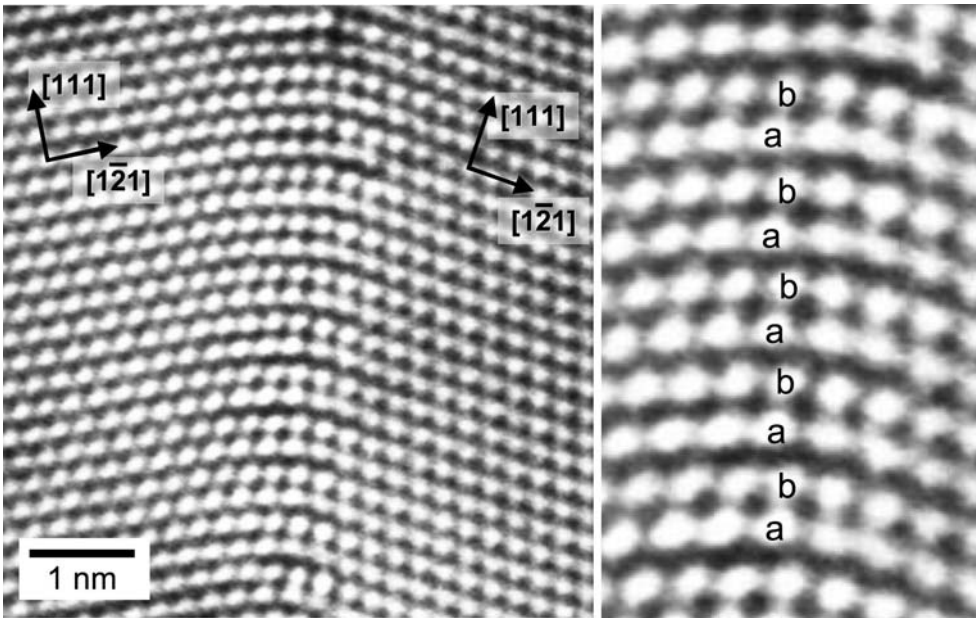

Fig. 2 HRTEM image of the dissociated grain boundary. The enlargement shows the …*abab*… stacking arrangement in the core region of the boundary

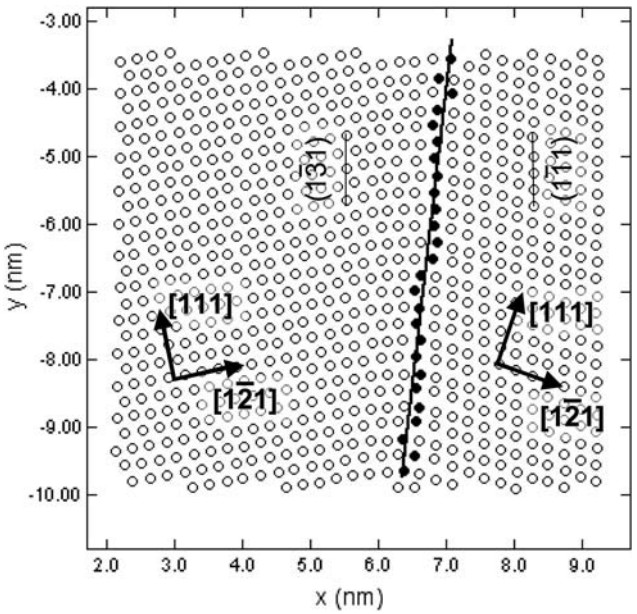

Fig. 3 Plot of the intensity peak positions extracted from the experimental image. The measured misorientation is 28.8 ± 0.5°. This angle approximately aligns $(1\bar{3}1)_{\text{left}}$ with $(1\bar{1}1)_{\text{right}}$. The marked positions indicate the edge of the boundary as discussed in the text. The boundary inclination measured from a line fit to these positions is 16.1° relative to [111] in the left crystal

Discussion

Relationship of the HCP interlayer to the interfacial geometry

Because HCP stacking is equivalent to introducing one stacking fault to every two {111} planes in a FCC crystal, we start by considering whether these stacking faults originate, as at lower misorientation angles, through the dissociation of crystal lattice dislocations. The question, then, is whether the boundary geometry—namely, its misorientation and inclination—is consistent with a distribution of crystal lattice dislocations at the appropriate density of one to every two {111} planes.

Consider a set of coplanar, crystal-lattice dislocations ($\mathbf{b} = 1/2\langle 110\rangle$). Taking the dislocation line direction ($\boldsymbol{\xi}$) to lie along the $[\bar{1}01]$ tilt axis, three types of perfect $1/2\langle 110\rangle$ dislocation lie on the (111) plane. One (±**BC** in Thompson's notation [15, 16]) is a pure screw dislocation, with **b** parallel with the $[\bar{1}01]$ tilt axis, and cannot contribute to the tilt misorientation. However, the remaining two types of dislocation (±**AB** and ±**AC**), which have **b** at ±60° with respect to $[\bar{1}01]$, possess both screw and edge components; thus, the edge components of these dislocations could accommodate the tilt provided both types of dislocation are present in equal numbers so that their oppositely signed screw components cancel (e.g., reference [17]).

Figure 4 illustrates schematically how the dissociation of such an array of dislocations into Shockley partial dislocations ($\mathbf{b} = 1/6\langle 112\rangle$) would produce an HCP interlayer. Here, 60° $1/2\langle 110\rangle$-type dislocations (**BA** and **CA**) are distributed at a spacing of one dislocation to every two (111) planes. The dislocations are dissociated into Shockley partial dislocations in the normal way: $\mathbf{BA} \rightarrow \mathbf{B}\boldsymbol{\delta} + \boldsymbol{\delta}\mathbf{A}$ and $\mathbf{CA} \rightarrow \mathbf{C}\boldsymbol{\delta} + \boldsymbol{\delta}\mathbf{A}$ [16]. This dissociation introduces a stacking fault on every other (111) plane, thereby yielding an …*abab*… stacking sequence in the region between the partial dislocations. The left side of the dissociated layer consists of 30° Shockley partial dislocations (**B**$\boldsymbol{\delta}$ and **C**$\boldsymbol{\delta}$), which have opposite screw components,

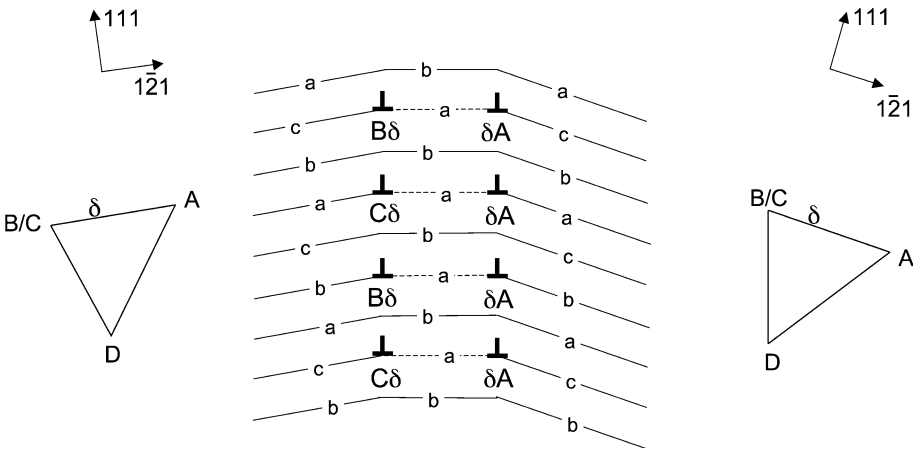

Fig. 4 Schematic showing dislocation arrangement forming interlayer of HCP. In this model, 60° 1/2⟨110⟩-type dislocations (**BA** and **CA**) are distributed at a spacing of one dislocation to every two {111} planes. These dislocations are dissociated into Shockley partial dislocations (**BA** → **B*δ*** + ***δ*A** and **CA** → **C*δ*** + ***δ*A**), creating faults on every other plane and resulting in an …*abab*… stacking sequence. The Thompson tetrahedra for the two crystals are shown along the [10$\bar{1}$] (B/C) projection. ***δ*A** is a pure edge, 90° dislocation; **B*δ*** and **C*δ*** are 30° dislocations with opposite screw components. Dashed lines indicate the stacking faults

while the right side consists of pure-edge, 90° Shockley partial dislocations (***δ*A**).

The Burgers vector density, **B**, at a grain boundary is related to the misorientation and inclination of the boundary through the Frank-Bilby equation (e.g., reference [18]):

$$\mathbf{B} = (\mathbf{I} - \mathbf{P}^{-1})\mathbf{v} \tag{1}$$

Here, **v** is a vector along the interface, expressed in the reference coordinate system (which we will take as the coordinates of the left crystal in Fig. 2), **P** is a rotation matrix describing the misorientation of the two crystals,[1] and **I** is the identity. We use this expression to solve for the misorientation and inclination that would give **B** of one 60° 1/2⟨110⟩ dislocation for every two (111) planes intersected by the interface (i.e., $\mathbf{B}/n_{111} = (1/8)[1\bar{2}1]$). Requiring **v** to be a periodic lattice translation vector, the equation is satisfied for $\mathbf{v} = 1/2[19, 10, 19]$ and $\mathbf{P}^{-1}\mathbf{v} = 1/2[13, 22, 13]$ (The corresponding boundary planes are (5, −19, 5) in the left crystal and (11, −13, 11) in the right crystal, which are inclined to $(1\bar{3}1)$ and $(1\bar{1}1)$ by 4.83° and 4.62°, respectively). The misorientation, which is given by the angle between these two vectors in the reference crystal, is 29.7°.

[1] **P** is computed from $\mathbf{P} = \mathbf{U}\mathbf{R}\mathbf{U}^{-1}$. For the geometry in this paper,

$$\mathbf{U} = \begin{pmatrix} 1/\sqrt{6} & 1/\sqrt{3} & -1/\sqrt{2} \\ -2/\sqrt{6} & 1/\sqrt{3} & 0 \\ 1/\sqrt{6} & 1/\sqrt{3} & 1/\sqrt{2} \end{pmatrix}$$

and

$$\mathbf{R} = \begin{pmatrix} \cos\theta & -\sin\theta & 0 \\ \sin\theta & \cos\theta & 0 \\ 0 & 0 & 1 \end{pmatrix}.$$

The boundary inclination, defined here as the angle of **v** with respect to [111], is half this amount, 14.85°. Although this dislocation arrangement produces an asymmetric tilt boundary, in that the boundary planes are different in the two adjacent crystals, the (111) planes in both crystals are rotated by equal amounts with respect to the boundary.

The misorientation and inclination predicted by this dislocation model compare well with the values measured from the experimentally observed boundary (misorientation: 28.8°; inclination: 16.1°). To estimate the significance of the difference between the observed misorientation and inclination and that of the idealized 29.7° model described above, we have computed from Eq. 1 the variation of **B** with inclination for both of these misorientations. **B** is plotted in terms of its [111] and $[1\bar{2}1]$ components, B_{111} and $B_{1\bar{2}1}$, in Fig. 5. These values are expressed as dimensionless quantities giving the magnitude of the Burgers vector per unit interface length. For the model (misorientation 29.7°, inclination 14.85°), $B_{1\bar{2}1}$ is 0.5126 and B_{111} is zero. For the observed boundary, $B_{1\bar{2}1}$ is 0.4972 and B_{111} is −0.0148. The magnitude of the difference in Burgers vector content for the observed and model boundaries multiplied by length of the observed boundary segment (about 60 Å) is 1.3 Å, which is still reasonably small compared with, say, the edge component of 60° 1/2⟨110⟩ dislocation (2.5 Å in gold). The small angular discrepancy may be a result of strains resulting from interactions with the nearby boundary junctions that can be seen Fig. 1. Within this limit, then, the misorientation and inclination of the observed boundary is consistent with the dislocation content of the model presented in Fig. 4, supporting the interpretation that the HCP interlayer forms through the dissociation of an array of individual crystal lattice dislocations.

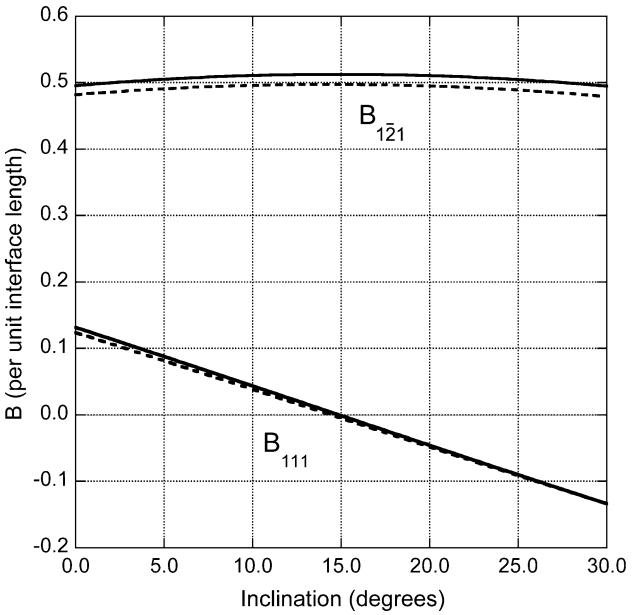

Fig. 5 Plot of the dependence of interfacial Burgers vector density, **B**, on inclination for misorientations of 29.7° (*solid line*) and 28.8° (*dashed*). Components of **B** along $[1\bar{2}1]$ and [111] are expressed per unit interface length. For a misorientation of 29.7° and inclination of 14.85°, $\mathbf{B}_{111}$ is zero and $\mathbf{B}_{1\bar{2}1}$ is 0.5126

Atomistic model

We constructed and relaxed an atomistic model to test further our interpretation of the interfacial dislocation structure. We used the embedded atom method (EAM) [19, 20] and employed a potential that was fit explicitly to the stacking fault energy of gold [11]. To construct the initial, *unrelaxed* configuration for this model we used the following procedure. We first joined two slabs of FCC material to an intermediate slab of HCP material oriented with $[2\bar{1}\bar{1}0]_{\mathrm{HCP}}$ parallel to the $[\bar{1}01]_{\mathrm{FCC}}$. Figure 6 illustrates these three slabs prior to being rotated and joined. We tried several widths for the initial HCP slab, ranging from the zero-width limit (i.e., simply joining the two FCC slabs with no starting HCP layer) to a maximum width of 30 Å. All of these starting configurations converged during relaxation to the same ending structure. Although the left and right FCC slabs were constructed with faces initially parallel to $(1\bar{3}1)$ and $(1\bar{1}1)$, respectively, we chose periodic boundary conditions to ensure that the overall interfacial inclination and misorientation would be consistent with a **B** of one 60° $1/2\langle 110\rangle$ dislocation for every two (111) planes intersected by the interface, as discussed in the previous section. In detail, the left and right FCC slabs were rotated by 10° and 19.7°, respectively, to join the $(10\bar{1}0)_{\mathrm{HCP}}$ faces on the two sides of the intermediate HCP layer. We chose these rotation angles so that $1/2[19, 10, 19]$ and $1/2[13, 22, 13]$, would be parallel in the two FCC crystals.

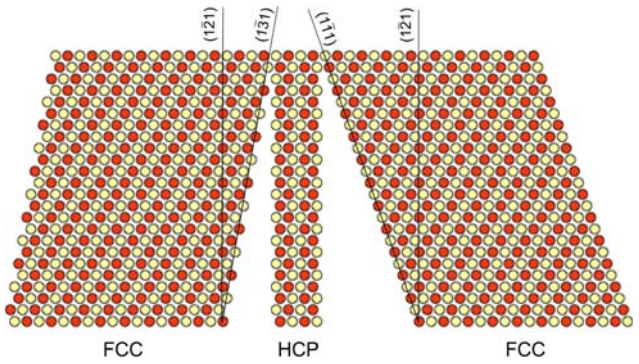

Fig. 6 Schematic illustrating an intermediate step in producing the initial configuration for the atomistic model

We applied a strain to the HCP layer to maintain continuity of the close-packed planes through the interface and then rotated the entire assembly so that periodic boundary conditions could be applied along the $1/2[19, 10, 19]$ and $1/2[13, 22, 13]$ directions. This construction gives an average interface inclination parallel to $(5, -19, 5)$ and $(11, -13, 11)$ planes in the left and right FCC crystals, respectively. We relaxed the structure using periodic boundary conditions in the directions parallel with the boundary and free surfaces at approximately 140 Å away from both sides of the boundary plane.

Figure 7a shows the relaxed model projected along a $[10\bar{1}]$ direction. The (111) planes bend gradually through a broad interfacial region where, as shown in the enlargement (Fig. 7b), the atoms are arranged in an …*abab*… stacking sequence. The atoms in Fig. 7a, b are shaded to indicate their relative depth along the $[10\bar{1}]$ axis. In a $\langle 110\rangle$ projection of a single crystal of FCC material, the atoms are at two depths that differ by the {220} interplanar spacing, $a/2\sqrt{2}$. Notably, the calculations predict a translation along the tilt-axis of $1/8[10\bar{1}]$, giving a planar offset of *half* the {220} spacing ($a/4\sqrt{2}$) (see Fig. 7c). This translation is a result of the alternating screw components of the dislocations present at the interface. As shown in Fig. 7b, c, the translation occurs at the *left* side of the dissociated interfacial layer, where the 30° Shockley partial dislocations (**B**$\boldsymbol{\delta}$ and **C**$\boldsymbol{\delta}$) are located, rather than at the right side with the 90° Shockley partial dislocations ($\boldsymbol{\delta}$**A**). Because **B**$\boldsymbol{\delta}$ and **C**$\boldsymbol{\delta}$ have oppositely signed screw components, there is no element of twist to the intergranular misorientation. However, the displacements due to these screw dislocations do combine to give a net displacement of $1/8[10\bar{1}]$ parallel to the tilt axis. For similar reasons, a translation of $1/8[10\bar{1}]$ is found in atomistic simulations of dissociated 90° {111}/{112} boundaries in Au, which form an intergranular layer of 9R stacked material [11]. As in the present case, the translation at the {111}/{112} boundary occurs at an array of closely spaced, 30° Shockley partial

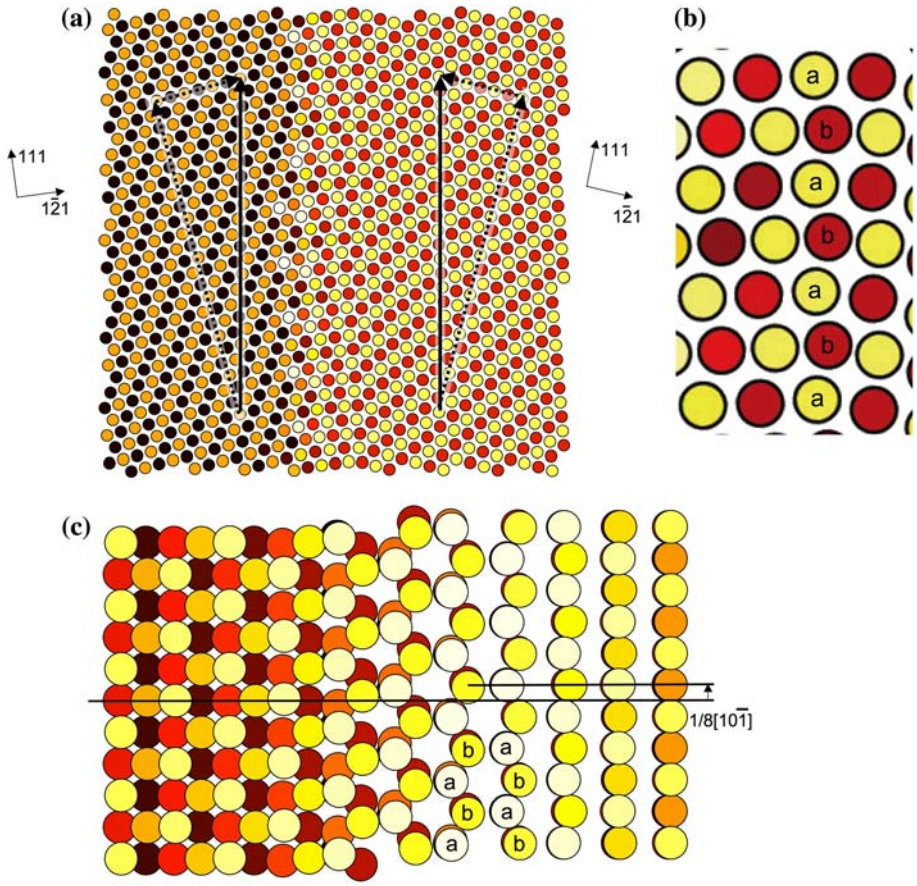

Fig. 7 Atomistic simulation of the boundary. **a** Projection along the $[10\bar{1}]$ tilt axis direction. The periodic lengths parallel with the interface, ½[19, 10, 19] and ½[13, 22, 13] in the left and right crystals, respectively, are shown. The different shading of the atoms indicates their relative height in the out-of-plane direction along the $[10\bar{1}]$ tilt axis. A translation of $1/8[10\bar{1}]$ in the out-of-plane direction occurs at the left side of the dissociated region. **b** An enlargement of the central dissociated region with the …*abab*… stacking of the HCP layer annotated. **c**. Projection along a direction orthogonal to the $[10\bar{1}]$ tilt axis (along the vertical direction of Fig. 4a). The locations of the *a* and *b* sites in the HCP intergranular layer are annotated. Away from the interface, the two FCC crystals are translated relative to each other by $1/8[10\bar{1}]$ along the tilt axis

dislocations terminating stacking faults emitted from the interface. Thus, even at a relatively high misorientation angle, the essential features of this boundary—namely its dissociation into HCP and its translation along the tilt axis—follow from the properties of the individual dislocations that constitute the interface.

Finally, we comment briefly on how the interfacial geometry affects the spacing of the close-packed planes within the HCP interlayer. Although the c/a ratio of the HCP layer is difficult to define precisely since the interfacial layer is quite narrow and the planes bend continuously as they cross the interface, we can nevertheless draw some general conclusions. First, to maintain continuity as they bend through the interface, the close-packed planes must be expanded to a larger separation than that of the {111} planes in the FCC bulk material. From the boundary conditions, the upper limit to this expansion is given by a factor of $1/\cos(\theta/2) = 1.034$. Furthermore, because the magnitude of the bending on the two sides of the interlayer is different, the expansion of the close-packed planes must be non-uniform and asymmetric across the thickness of the layer, being smallest at the left side of the layer, where the bending is least, and largest at the right side, where the bending is the most. Qualitatively, the difference in bending on the two sides of the layer occurs because the edge components of the 90° partial dislocations at the right side of the layer are larger than those of the 30° dislocations at the left.

Relationship to dissociated structures at higher misorientation: HCP at the 80.63° ⟨110⟩ {353} ($\Sigma = 43$) symmetric tilt boundary

We now turn to a second question: how is this structure related to the dissociated intergranular layers that have been observed at higher misorientations? Because hexagonal close packing is equivalent to the highest possible density of stacking faults in an FCC structure, the 29.7° boundary likely represents an upper limit of misorientation for which such grain boundary structures can be meaningfully described in terms of the dissociation of individual $1/2\langle 110\rangle$ crystal lattice dislocations. Nevertheless, because dense arrays of stacking faults are also found at many boundaries at yet higher misorientation angles, it is interesting to consider how the present boundary is related to these other boundaries. Of specific relevance to our discussion is the 80.63° ⟨110⟩{353} ($\Sigma = 43$) symmetric tilt boundary, since this boundary also dissociates to form an interlayer of HCP material [10–12].

It is useful to analyze the structures of such dissociated high angle boundaries by modeling the interfaces as dense arrays of individual Shockley partial dislocations (rather than full crystal lattice dislocations). In particular, the pattern of faults at symmetric ⟨110⟩ tilt boundaries with misorientations in the range of 50.5° to 109.5° can be predicted by modeling the interfaces as sets of 90° (**Aδ**) and 30° (**Bδ** and **Cδ**) Shockley partial dislocations that are distributed on adjacent, close-packed planes [11, 12]. The idea behind this analysis is that the misorientation produced by the array consists of two components: one component due to the twinning operation of the partial dislocations and a second component due to the net Burgers vector of the dislocation array. For instance, a periodic distribution of partial dislocations consisting of equal numbers of **Aδ**, **Bδ**, and **Cδ** would have zero net Burgers vector but would still rotate the crystal lattice (by 70.53° about ⟨110⟩) by twinning it, as was noted by Dash and Brown [21] in early studies of annealing twins in FCC materials.

The relationship between the net Burgers vector, $\mathbf{B}^*$, of this array and the interfacial geometry is [11]:

$$\mathbf{B}^* = \mathbf{v} - \mathbf{P}_{\text{twin}}\mathbf{v}' \tag{2}$$

where $\mathbf{v}$ and $\mathbf{v}'$ are vectors along the interface expressed in the untwinned and twinned crystals, respectively, and $\mathbf{P}_{\text{twin}}$ describes the twinning rotation.[2] Representing the total rotation between the two grains by the rotation matrix $\mathbf{P}$, as before, Eq. 2 can be rewritten in a form similar to the Frank-Bilby equation:

$$\mathbf{B}^* = \left(\mathbf{I} - \mathbf{P}_{\text{twin}}\mathbf{P}^{-1}\right)\mathbf{v} \tag{3}$$

For symmetric ⟨110⟩ tilt boundaries, this equation can be solved to determine the distribution of Shockley partial dislocations describing a given misorientation and inclination. The symmetric 80.63° ⟨110⟩{353} ($\Sigma = 43$) boundary is a limiting case in this framework since it is composed of a 1:1 ratio of 90° (**Aδ**) and 30° (**Bδ** and **Cδ**) partial dislocations.[3] As has been discussed previously [11, 12], if these dislocations are distributed in a repeat sequence of …**Aδ Bδ Aδ Cδ**…, separation of the 90° and 30° dislocations produces an HCP interlayer by forming a stacking fault on alternating {111} planes. Such a structure is consistent with atomistic simulations of this interface [10] and further supported by HRTEM observations of a boundary in Au near this misorientation and inclination [12].

The dislocation arrangements at the 29.7° boundary and the 80.63° {353} boundary are closely related. In both cases, the boundaries are composed of walls of 90° and 30° Shockley partial dislocations. The partial dislocations in these walls are each distributed one to every 2 {111} planes. The essential difference between the boundaries is the following. At the 29.7° boundary, the 90° and 30° partial dislocations have the same sign and are paired on the same plane to form full lattice dislocations (separated by a stacking fault). At the 80.63° boundary, the 90° and 30° partial dislocations are oppositely signed and sit on alternate planes.

We illustrate the relationship between these two boundaries schematically in Fig. 8. In particular, one could imagine converting between these two boundaries by transforming the array of 90° partial dislocations through a suitable dislocation reaction. This notion is illustrated in Fig. 8a. Here the left side of Fig. 8a shows the array of dissociated 1/2⟨110⟩ dislocations that describe the 29.7° boundary and its HCP interlayer. We now imagine sweeping into the crystal a wall of 90° partial dislocations (**Aδ**), distributed with one to each adjacent {111} plane, and allowing these dislocations to react with the oppositely signed 90° partial dislocations (**δA**) at the right side of the 29.7° boundary. As it passes through the right crystal, the **Aδ**-wall reorients the crystal by shearing each {111} plane by a vector of type 1/6⟨112⟩. Once the **Aδ** dislocations reach the right side of the 29.7° boundary, half of the dislocations cancel with the **δA** dislocations already at the interface resulting in a sequence of *unpaired* partial dislocations, …**Aδ Bδ Aδ Cδ** …, along the interface. This operation, thus, produces the same sequence of partial dislocations as at the symmetric $\Sigma = 43$ boundary.

This dislocation reaction can be analyzed quantitatively using Eqs. 1 and 3. The Burgers vector density (normalized per {111} plane intersected by the interface) for the 29.7° boundary is $\mathbf{B} = \frac{1}{8}[1\bar{2}1]$. The array of **Aδ** dislocations, distributed at 1 per {111} plane, has $\mathbf{B}^* = \frac{1}{6}[\bar{1}2\bar{1}]$. Adding these two arrays of dislocations gives $\mathbf{B} + \mathbf{B}^* = \frac{1}{24}[\bar{1}2\bar{1}]$. This is the Burgers vector density (per {111} plane) that is produced by the Shockley partial sequence: …**Aδ Bδ Aδ Cδ** …. Solving Eq. 3 for this Burgers vector density and taking $\mathbf{v}$ to be a periodic lattice translation vector gives $\mathbf{v} = \frac{1}{2}[5\bar{6}5]$ and $\mathbf{P}^{-1}\mathbf{v} = \frac{1}{2}[5\bar{6}5]$ ($\mathbf{P}^{-1}\mathbf{v}$ is the interface vector in the rotated, right crystal). The interface planes are thus $(3\bar{5}3)/(\bar{3}\bar{5}\bar{3})$ and the misorientation about the $[10\bar{1}]$ axis is 80.63°, which is the symmetric $\Sigma = 43$ boundary. In forming this symmetric configuration from the 29.7° boundary, the inclination therefore rotates by 19.9° in the anti-clockwise direction (i.e., in the left crystal going from a inclination along [19, 10, 19] to an inclination along [565]).

[2] For the geometry in this paper, $\mathbf{P}_{\text{twin}} = \frac{1}{3}\begin{pmatrix} 2 & -2 & -1 \\ 2 & 1 & 2 \\ -1 & -2 & 2 \end{pmatrix}$.

[3] For the $\Sigma = 43$, $\theta = 80.63°$ $(3\bar{5}3)/(\bar{3}\bar{5}\bar{3})$ boundary, $\mathbf{v} = \frac{1}{2}[5, 6, 5]$. From Eq. 3, $\mathbf{B}^* = \frac{1}{3}[\bar{1}2\bar{1}]$. As discussed in reference [11], requiring that $\mathbf{B}^*$ be composed of Shockley partial dislocations distributed one to each of the 8 {111} planes crossed by $\mathbf{v}$ gives a distribution of 4 **Aδ**, 2 **Bδ**, and 2 **Cδ**.

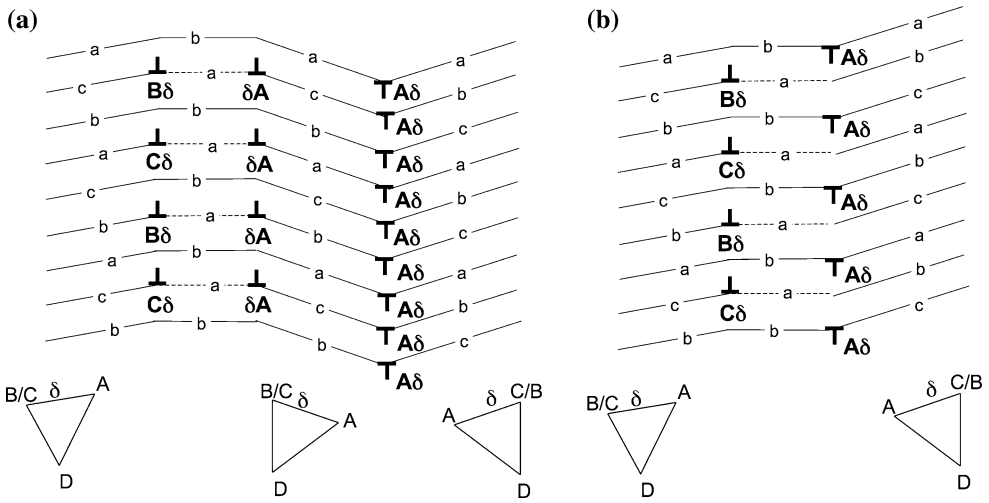

Fig. 8 Schematic illustrating the inter-relationship between the two HCP boundaries. **a** The left-most boundary is the same as shown in Fig. 3. On the right, one imagines a wall of 90° Shockley partial dislocations (**Aδ**), distributed one to every {111} plane, sweeping in from the right. These dislocations reverse the stacking on the right side of the wall. In (**b**) the array of **Aδ** dislocations has reached the right side of the interface, eliminating the **δA** dislocations that had formed the right side of the HCP slab and leaving an **Aδ** dislocation on the remaining planes. The resulting arrangement of *un-paired* partial dislocations is the same as that forming ⟨110⟩ $\Sigma = 43$ boundary [11, 12]

Conclusions

The analysis here helps to link our understanding of low- and high-angle grain boundary structure. In this particular case, we have shown how the dissociation of a dense array of perfect crystal lattice dislocations into partial dislocations produces an interfacial layer of hexagonal close packed material and how this dislocation array is related to the partial dislocations that produce HCP at the high-angle $\Sigma = 43$ boundary. The success in connecting these two boundaries of quite different misorientation suggests that similar analyses in terms of individual partial dislocations may have general utility in unifying our understanding of FCC boundary structure as a function of misorientation.

Acknowledgements Sandia is a multi-program laboratory operated by Sandia Corporation, a Lockheed Martin Company, for the United States Department of Energy, National Nuclear Security Administration, under Contract DE-AC04-94AL85000. This work was supported in part by the DOE Office of Basic Energy Science, Division of Materials Sciences. The authors acknowledge helpful comments from J. Sugar, S. Foiles, and the anonymous reviewer.

Appendix A: Analysis of a step at the {111}/{131} interface

In the main text, we have analyzed the defect content of the interface with reference to one of the two adjacent single crystals. We chose this approach because it directly addresses the origin of the stacking fault pattern and its relationship to boundaries at other misorientations. However, because the boundary in this paper is vicinal to {111}/{131}, it is also instructive to analyze the interface relative to a reference frame in which these planes are aligned. This complementary analysis approach, which we discuss below, provides further insight concerning the nature of the interface at the facet length scale.

For this analysis, we adopt a *coherent* reference frame following an approach used previously for boundaries in FCC metals vicinal to {111}/{121} [22, 23]. The dichromatic pattern representing this strained reference state is shown in Fig. 9. Here, $(\bar{1}3\bar{1})$ and $(\bar{1}1\bar{1})$ are rotated into

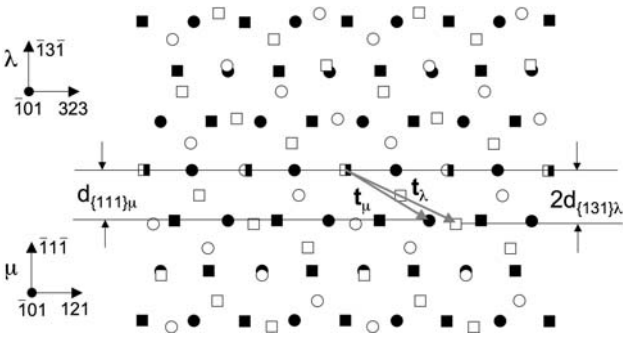

Fig. 9 Dichromatic pattern for the coherently strained reference state. $(\bar{1}3\bar{1})$ and $(\bar{1}1\bar{1})$ are rotated into alignment ($\theta = 29.496°$) and periodic lengths parallel to the interface in the upper (λ) and lower (μ) crystals $(1/2[323]_\lambda$ and $[121]_\mu)$ are strained into coherency. The analyzed disconnection can be envisioned as the difference between two lattice translation vectors, $\mathbf{t}_\lambda = [101]$ and $\mathbf{t}_\mu = \frac{1}{2}[211]$. The difference in step heights (2 $(\bar{1}3\bar{1})$ planes λ and 1 $(\bar{1}1\bar{1})$ plane in μ) gives a component of Burgers vector that is perpendicular to the $(\bar{1}3\bar{1})_\lambda // (\bar{1}1\bar{1})_\mu$ terrace

alignment ($\theta = 29.496°$) and periodic lengths parallel to the interface in the upper (λ) and lower (μ) crystals $(1/2[323]_\lambda$ and $[121]_\mu)$ are strained into coherency. The matrix defining this coherent reference state, $\mathbf{P}_{coh}$, is given by:

$$\mathbf{P}_{coh} = \mathbf{P}_{rel}\mathbf{U}_\mu \mathbf{A} \mathbf{U}_\mu^{-1} \tag{4}$$

$\mathbf{P}_{rel}$ relates the coordinate frames of the two relaxed and unstrained crystals, $\mathbf{A}$ describes the uniaxial compression of μ to bring it into coherency with λ (in unit orthogonal coordinates), and $\mathbf{U}_\mu$ converts from unit orthogonal coordinates to μ crystal coordinates:

$$\mathbf{P}_{rel} = \frac{1}{2\sqrt{33}}\begin{pmatrix} 5+\sqrt{33} & 4 & 5-\sqrt{33} \\ -4 & 10 & -4 \\ 5-\sqrt{33} & 4 & 5+\sqrt{33} \end{pmatrix}$$

$$\mathbf{A} = \begin{pmatrix} \frac{1}{2}\sqrt{\frac{11}{3}} & 0 & 0 \\ 0 & 1 & 0 \\ 0 & 0 & 1 \end{pmatrix}; \tag{5}$$

$$\mathbf{U}_\mu = \frac{1}{\sqrt{6}}\begin{pmatrix} 1 & -\sqrt{2} & -\sqrt{3} \\ 2 & \sqrt{2} & 0 \\ 1 & -\sqrt{2} & \sqrt{3} \end{pmatrix}$$

As noted in the results sections, the observed section of boundary consists of two terraces that are separated by a step-like defect (or "disconnection" in the terminology of Hirth [24], which emphasizes the dual roles of step and dislocation content of such defects). By constructing a circuit around the disconnection, and then mapping this circuit into the coherent reference frame, the topological properties of the defect can be established. Figure 10 shows the intensity peak positions extracted from the HRTEM image of the dissociated boundary. This is the same data as in Fig. 3 of the paper, but here the data are rotated so that $(\bar{1}3\bar{1})$ and $(\bar{1}1\bar{1})$ are horizontal to better highlight the step and to allow comparison with Fig. 9.

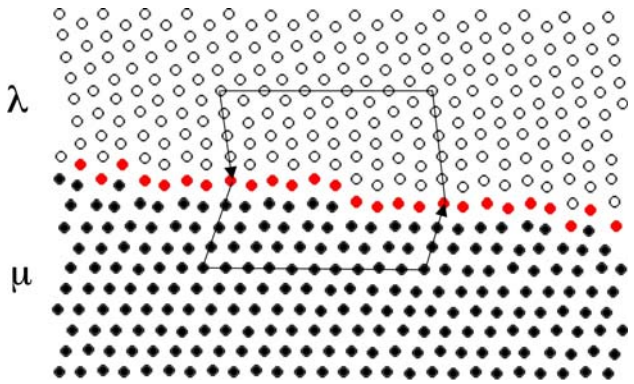

Fig. 10 Circuit analysis of the observed interfacial disconnection. The data are the same as in Fig. 3, but is rotated here by 90°

Denoting the circuits in the upper and lower crystals as C_λ and C_μ, respectively, the Burgers vector associated with this disconnection is given by:

$$\mathbf{b} = -\left(C_\lambda + \mathbf{P}_{coh} C_\mu\right) \tag{6}$$

Resolving $\mathbf{b}$ into edge components parallel and normal to the terrace gives: $b_{||} = 0.3020a$ and $b_n = -0.0256a$. The defect also possesses a screw component of $b_{screw} = \pm 0.3535a$. The step heights in the upper and lower crystals are $-2d_{131} = -0.603a$ and $-d_{111} = -0.577a$, respectively. As illustrated in Fig. 9, this defect can be envisioned as the difference between two lattice translation vectors, $\mathbf{t}_\lambda = [101]$ and $\mathbf{t}_\mu = \frac{1}{2}[211]$ (note: $\mathbf{b} = \mathbf{t}_\lambda - \mathbf{P}_{coh}\mathbf{t}_\mu$).

A periodic array of such disconnections would rotate both the boundary inclination and crystal misorientation from $(\bar{1}3\bar{1})_\lambda // (\bar{1}1\bar{1})_\mu$ due to the step and dislocation content of the defects. Pond et al. have derived the relationships for the interface inclination and misorientation when disconnections are spaced at the separation required to fully accommodate the interfacial coherency strain [25]. Using the expressions in Appendix B of reference [25], we compute that an array of disconnections of the type observed here would accommodate the coherency strain at the $(\bar{1}3\bar{1})_\lambda // (\bar{1}1\bar{1})_\mu$ interface when distributed at a separation of $L = 7.166a$ (an equal distribution of positive and negative screw components would be required to cancel any twist). At this spacing, the normal component of the Burgers vector of the disconnections adds 0.206° to the crystal misorientation, bringing the total misorientation to 27.702°. Moreover, the step components of the disconnections rotate the macroscopic boundary inclination from $(\bar{1}3\bar{1})_\lambda // (\bar{1}1\bar{1})_\mu$ by 4.83° in λ and 4.62° in μ (both in the clockwise direction). This misorientation and macroscopic boundary inclination are equivalent to that computed in section 1 of the discussion using the Frank-Bilby equation for a Burgers vector density of one 60° $1/2\langle 110\rangle$ dislocation for every two (111) planes intersected by the interface. This analysis, then, gives a microscopic picture of the relationship between the macroscopic geometric parameters of the interface and its specific atomic-scale defects.

References

1. Krakow W, Smith DA (1987) Ultramicroscopy 22:47
2. Merkle KL (1990) Colloq Phys C1 51:251
3. Ernst F, Finnis MW, Hofmann D, Muschik T, Schönberger U, Wolf U, Methfessel M (1992) Phys Rev Lett 66:991
4. Wolf U, Ernst F, Muschik T, Finnis MW, Fischmeister HF (1992) Philos Mag A 66:991
5. Merkle KL (1994) J Phys Chem Solids 55:991
6. Medlin DL, Campbell GH, Carter CB (1998) Acta Mater 46:5135
7. Radetic T, Lançon F, Dahmen U (2002) Phys Rev Lett 89:85502
8. Brown JA, Mishin Y (2007) Phys Rev B 76:134118

9. Tschopp MA, Tucker GJ, McDowell DL (2007) Acta Mater 55:3959
10. Rittner JD, Seidman DN (1996) Phys Rev B 54:6999
11. Medlin DL, Foiles SM, Cohen D (2001) Acta Mater 49:3689
12. Lucadamo G, Medlin DL (2003) Science 300:1272
13. Jenkins ML (1972) Philos Mag 36:747
14. Balk TJ, Hemker KJ (2001) Philos Mag A 81:1507
15. Thompson N (1953) Proc Phys Soc Sect B 66B:481
16. Hirth JP, Lothe J (1992) Theory of dislocations. Krieger Publishing Company, Malabar, FL
17. Read WT (1953) Dislocations in crystals. McGraw-Hill, New York, p 17
18. Sutton AP, Balluffi RW (1995) Interfaces in crystalline materials. Clarendon Press, Oxford, p 70
19. Daw MS, Baskes MI (1983) Phys Rev Lett 50:1285
20. Daw MS, Baskes MI (1984) Phys Rev B 29:6443
21. Dash S, Brown N (1963) Acta Metall 35:1067
22. Medlin DL, Cohen D, Pond RC (2003) Philos Mag Lett 83(4):223
23. Pond RC, Medlin DL, Serra A (2006) Philos Mag 86(29–30): 4667
24. Hirth JP (1994) J Phys Chem Solids 55:985
25. Pond RC, Celotto S, Hirth JP (2003) Acta Mater 51:5385